Stochastic Models in Coordinate-Delay Synthetic Aperture Radar Imaging

Mikhail Gilman[1,*], Semyon Tsynkov[1]
[1]Department of Mathematics, North Carolina State University, Raleigh, North Carolina, USA
[*]Email: mgilman@ncsu.edu

Abstract

We build stochastic models for synthetic aperture radar (SAR) imaging of targets that exhibit delayed scattering. Detection of scattering delay in SAR is hindered by the range-delay ambiguity, and the stochasticity of scattering adds uncertainty to the result. Using Monte-Carlo simulations, we obtain ensembles of coordinate-delay SAR images of instantaneous and delayed targets. Then, we explore the separation of likelihood-based metrics for those ensembles.

Keywords: SAR, range-delay ambiguity, Monte-Carlo simulation, Hellinger distance

1 Coordinate-delay SAR

By detecting and analyzing the scattering delay, we can learn important geometrical information about radar targets such as the presence of cavities, their internal structure, and characteristic size. Following [1], we will consider targets for which the relation between the incident u^{i} and scattered u^{s} fields is local in space and non-local in time. It is rendered by the spatio-temporal reflectivity function $\nu(t_{\boldsymbol{z}}, \boldsymbol{z})$:

$$u^{\mathrm{s}}(t, \boldsymbol{z}) = \int_0^\infty u^{\mathrm{i}}(t - t_{\boldsymbol{z}}, \boldsymbol{z}) \nu(t_{\boldsymbol{z}}, \boldsymbol{z})\, dt_{\boldsymbol{z}}. \quad (1)$$

The coordinate-delay SAR (cdSAR) image is built from a series of scattering events with signals transmitted and received from the locations $\boldsymbol{x}^n$ spaced over the synthetic aperture: $I(t_{\boldsymbol{y}}, \boldsymbol{y}) = \sum_n \int \overline{P(t - t_{\boldsymbol{y},n})} u^{\mathrm{s}}(t, \boldsymbol{x}^n)\, dt$. In this formula, $t_{\boldsymbol{y},n} = t_{\boldsymbol{y}} + 2|\boldsymbol{x}^n - \boldsymbol{y}|/c$ is the sum of scattering and propagation delays, and $\overline{P}$ is the complex conjugate of the frequency modulated transmitted pulse: $P(t) = e^{-i\omega_0 t} e^{-iBt^2/(2\tau)}$, $|t| \leqslant \tau$, where B and τ are pulse bandwidth and duration, respectively. In the linearized setting (1), the image is given by a convolution operator

$$I(t_{\boldsymbol{y}}, \boldsymbol{y}) = \int_0^\infty dt_{\boldsymbol{z}} \int d\boldsymbol{z}\, \nu(t_{\boldsymbol{z}}, \boldsymbol{z}) W(t_{\boldsymbol{y}}, \boldsymbol{y}; t_{\boldsymbol{z}}, \boldsymbol{z}), \quad (2)$$

with the kernel defined as

$$\frac{W}{N\tau} = e^{-2i\xi\omega_0/B} \operatorname{sinc}\xi \int_{-1/2}^{1/2} e^{2i\eta s} e^{i\kappa\xi_{\mathrm{r}} s^2} ds. \quad (3)$$

In (3), $\operatorname{sinc} x = \sin(x)/x$, $\xi_{\mathrm{r}} = B(y_2 - z_2)\sin\theta/c$, $\xi_{\mathrm{d}} = B(t_{\boldsymbol{y}} - t_{\boldsymbol{z}})/2$, $\xi = \xi_{\mathrm{r}} + \xi_{\mathrm{d}}$, $\kappa = \varphi_T^2\omega_0/B$, N is the number of pulses per the synthetic array, $\eta = \varphi_T\omega_0(y_1 - z_1)\sin\theta/c$, φ_T is the angular aperture size, θ is the incident angle, and the indices 1 and 2 denote the cross-range and range coordinates, respectively.

The range-delay ambiguity is due to a combination of range- and time-dependent terms in ξ, and is controlled by the value of κ. If $\kappa \to 0$, then the integral in (3) is just $\operatorname{sinc}\eta$. Hence, the dependence of W on ξ_{r} disappears and the two terms in ξ cannot be separated. In this case, we see that the cdSAR image (2) will be constant along the lines $y_2 \sin\theta + ct_{\boldsymbol{y}}/2 = \text{const}$.

2 Stochastic scatterers and cdSAR

Speckle in SAR [2] is seen as rapid and strong variations of the observed reflectivity of an extended scatterer whereas the true quantities of interest vary gradually and smoothly. Due to a large parameter ω_0/B in the exponent in (3), the kernel in (2) oscillates rapidly and thus emphasizes the singularities of ν in the directions z_2 and $t_{\boldsymbol{z}}$. Typically, the reflectivity is rough on the scale of the wavelength $\lambda_0 = 2\pi c/\omega_0$, while the size of the resolution cell in range is $\sim c/B \gg \lambda_0$. The following stochastic model proved effective in standard SAR [2]. It simulates a large number of point scatterers that are randomly positioned inside each resolution cell and represent the singularities of ν:

$$\nu_{\mathrm{b}}(t_{\boldsymbol{z}}, \boldsymbol{z}) = \delta(t_{\boldsymbol{z}})\mu_{\mathrm{b}}(\boldsymbol{z}). \quad (4)$$

In (4), $\mu_{\mathrm{b}}(\boldsymbol{z})$ is a two-dimensional circular Gaussian white random field:

$$\langle \mu_{\mathrm{b}}(\boldsymbol{z}) \rangle = 0, \ \langle \overline{\mu_{\mathrm{b}}(\boldsymbol{z})} \mu_{\mathrm{b}}(\boldsymbol{z}') \rangle = \sigma_{\mathrm{b}}^2 \delta(\boldsymbol{z} - \boldsymbol{z}'). \quad (5)$$

In (5), σ_{b}^2 is a deterministic parameter that characterizes the average reflectivity of a homogeneous extended scatterer.

As an extension to (4)–(5), we introduce two new stochastic scatterer models: ν_t is a delayed point scatterer and ν_s is an inhomogeneous in-

stantaneous scatterer:

$$\nu_t(t_{\boldsymbol{z}}, \boldsymbol{z}) = \mu_t(Bt_{\boldsymbol{z}}/2)\delta(\boldsymbol{z} - \boldsymbol{z}_{\rm d}), \tag{6}$$

$$\nu_s(t_{\boldsymbol{z}}, \boldsymbol{z}) = \mu_s\big(B(z_2 - z_{\rm d2})\sin\theta/c\big) \cdot \delta(t_{\boldsymbol{z}})\delta(z_1 - z_{\rm d1}), \tag{7}$$

where $\boldsymbol{z}_{\rm d} = (z_{\rm d1}, z_{\rm d2}, 0)$ is the reference location of the inhomogeneity. In (6)–(7), $\mu_{s,t}(\xi)$ are inhomogeneous one-dimensional circular Gaussian white random processes described by

$$\big\langle \overline{\mu_{s,t}(\xi)}\mu_{s,t}(\xi')\big\rangle = \sigma^2_{s,t}F(\xi)\delta(\xi - \xi'),$$

where σ_s^2 and σ_t^2 are the averaged reflectivities of the corresponding scatterers, $0 \leqslant F \leqslant 1$, and we choose $F(\xi) = 0$ for $\xi < 0$ to account for the causality in (1). The justification for introducing stochasticity for ν_t may be seen in the presence of multiple cavity eigenmodes and/or multipath reflection. The form of F will characterize the scatterer: we choose $F(\xi) = 1$ for $0 \leqslant \xi \leqslant \xi_{\max}$ and zero otherwise, where $\xi_{\max}$ describes the maximum scattering delay.

The reflectivities ν_s and ν_t of (6)–(7) are built so that they produce similar cdSAR images when the range-delay ambiguity is not resolved, e.g., when $\kappa \to 0$ (Section 1). Hence, we will use (6)–(7) to explore our ability to distinguish between the instantaneous and delayed scatterers. The background (clutter) (4)–(5) is added to (6)–(7) to create the overall reflectivity

$$\nu = \nu_{\rm b} + \nu_t \quad \text{or} \quad \nu = \nu_{\rm b} + \nu_s. \tag{8}$$

3 Monte-Carlo simulations

The autocorrelation of a cdSAR image can be obtained by substituting models (8) with (4)–(7) into (2) and subsequent averaging. Then, for given intensities $\sigma^2_{\rm b}$, σ^2_s, and σ^2_t, we can use the Monte-Carlo method to manufacture ensembles of cdSAR images (i.e., arrays of pixel values $\mathbf{Q}$) due to one of the two models in (8) with the corresponding multivariate Gaussian statistics. Optionally, we can add to the result an uncorrelated circular Gaussian term to represent the noise. If, on the other hand, we have an array $\mathbf{Q}$ randomly generated as above or obtained by observations, then we can use the same statistics to calculate the probability density function (pdf) of $\mathbf{Q}$ due to either of these models. Denoting these likelihood functions by $p_s(\mathbf{Q}) \equiv p_s(\mathbf{Q}; \sigma^2_{\rm b}, \sigma^2_s)$ and $p_t(\mathbf{Q}) \equiv p_t(\mathbf{Q}; \sigma^2_{\rm b}, \sigma^2_t)$, we calculate

$$\breve{p}_t(\mathbf{Q}) = \max_{\sigma^2_{\rm b}, \sigma^2_t} p_t(\mathbf{Q}), \quad \breve{p}_s(\mathbf{Q}) = \max_{\sigma^2_{\rm b}, \sigma^2_s} p_s(\mathbf{Q}).$$

Other parameters, such as $\boldsymbol{z}_{\rm d}$, can be added to the set of optimization variables.

Although the multivariate Gaussian models can yield any data with nonzero pdf, we expect that on average, $\breve{p}_t(\mathbf{Q}) \geqslant \breve{p}_s(\mathbf{Q})$ for the data produced from the first model in (8), and $\breve{p}_t(\mathbf{Q}) \leqslant \breve{p}_s(\mathbf{Q})$ for the second one. In order to characterize the separation between the two models numerically, we use the Hellinger distance $H[f, g]$ between two pdfs, $f(x)$ and $g(x)$, defined as $H[f, g] = \frac{1}{2}\int \big(\sqrt{f(x)} - \sqrt{g(x)}\big)^2\, dx$, see [3]. In the limiting cases, $H[f, g] = 1$ when f and g are completely disjoint, and $H[f, f] = 0$.

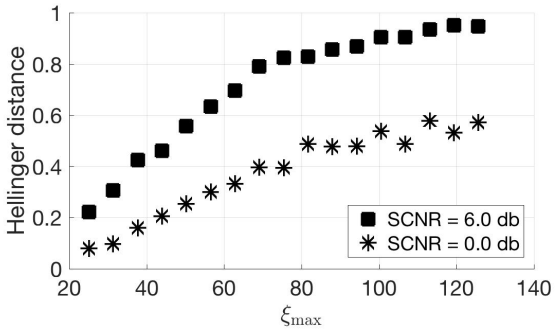

Figure 1: Plot of the Hellinger distance vs. $\xi_{\max}$.

We calculate the Hellinger distance between the pdfs of $\log\big(\breve{p}_t(\mathbf{Q})/\breve{p}_s(\mathbf{Q})\big)$ for the ensembles generated according to the two models in (8). Figure 1 plots this distance for two different values of signal to clutter and noise ratio (SCNR) and $\kappa = 1/4$. We can see that with high SCNR and large scattering delays $\xi_{\max}$, the models in (8) are safely distinguishable.

Acknowledgements

This material is based upon work supported by the US Air Force Office of Scientific Research under award number FA9550-17-1-0230.

References

[1] Matthew Ferrara, Andrew Homan, and Margaret Cheney, Hyperspectral SAR, *IEEE Transactions on Geoscience and Remote Sensing*, **55(3)** (2017), pp. 1–14.

[2] Chris Oliver and Shaun Quegan, *Understanding Synthetic Aperture Radar Images*, Artech House, Boston, 1998.

[3] David Pollard, *A User's Guide to Measure Theoretic Probability*, Cambridge University Press, 2002.